

Research Article

<https://doi.org/10.1631/jzus.A2300340>

Efficient reliability analysis via a nonlinear autoregressive multi-fidelity surrogate model and active learning

Yifan LI, Yongyong XIANG, Luojie SHI, Baisong PAN✉

College of Mechanical Engineering, Zhejiang University of Technology, Hangzhou 310023, China

Abstract: For complex engineering problems, multi-fidelity modeling has been used to achieve efficient reliability analysis by leveraging multiple information sources. However, most methods require nested training samples to capture the correlation between different fidelity data, which may lead to a significant increase of low-fidelity samples. In addition, it is difficult to build accurate surrogate models because current methods do not fully consider the nonlinearity between different fidelity samples. To address these problems, a novel multi-fidelity modeling method with active learning is proposed in this paper. Firstly, a nonlinear autoregressive multi-fidelity Kriging (NAMK) model is used to build a surrogate model. To avoid introducing redundant samples in the process of NAMK model updating, a collective learning function is then developed by a combination of a U-learning function, the correlation between different fidelity samples, and the sampling cost. Furthermore, a residual model is constructed to automatically generate low-fidelity samples when high-fidelity samples are selected. The efficiency and accuracy of the proposed method are demonstrated using three numerical examples and an engineering case.

Key words: Reliability analysis; Multi-fidelity surrogate model; Active learning; Nonlinearity; Residual model

1 Introduction

Reliability analysis plays a critical role in engineering design, as it aims to assess the probability of system failure with respect to specific performance criteria, considering the presence of various uncertainties (Echard et al., 2013). Generally, the failure probability can be calculated by a multi-dimensional integral

$$P_f = \int_{G(\mathbf{x}) < 0} f_{\mathbf{x}}(\mathbf{x}) d\mathbf{x}, \quad (1)$$

where $\mathbf{x} = [x_1, \dots, x_n]^T$ denotes all random input variables, $f_{\mathbf{x}}(\mathbf{x})$ is the joint probability density function of \mathbf{x} , and $G(\mathbf{x})$ represents the limit state function.

In practical engineering scenarios, the analytical solution of the above integral may not be obtained

because limit state functions are usually implicit (Schuëler and Pradlwarter, 2007). The Monte Carlo simulation (MCS) method is a robust tool to deal with this problem. Nonetheless, a key limitation of MCS is the need for extensive limit state function evaluations to precisely estimate failure probabilities. Especially for complex problems which need finite element analysis, the total computational budget is unaffordable (Lelièvre et al., 2018). Some novel sampling methods, for example, importance sampling (IS) (Melchers, 1990; Papaioannou et al., 2016) and subset simulation (SS) (Song et al., 2009; Li and Cao, 2016), have been developed to enhance the efficiency of MCS, but they still require a substantial number of calls to the limit state function to obtain the failure probability with a satisfactory level of accuracy. Most probable point-based (MPP-based) methods, such as the first-order reliability method (FORM) (Hohenbichler and Rackwitz, 1982) and second-order reliability method (SORM) (Kiureghian and Stefano, 1991), are frequently used to perform effective reliability analysis. However, these methods may have large errors when dealing with scenarios involving multiple MPPs or highly nonlinear limit state functions (Gavin and Yau, 2008).

✉ Baisong PAN, panbsz@zjut.edu.cn

Moment-based methods (Hong, 1996; Zhang and Pandey, 2013), which reconstruct the actual limit state probability density function from statistical moments derived from sampling, depend heavily on the choice of a suitable statistical model for their accuracy.

Recently, surrogate models have gained widespread popularity in reliability analysis, primarily due to their capability to handle problems characterized by complex implicit limit state functions. These models enable numerous simulation runs at a limited computational cost, facilitating failure probability evaluations (Wang et al., 2021; Aldosary et al., 2018). Representative surrogate models include response surface methodology (RSM) (Rajashekhar and Ellingwood, 1993; Goswami et al., 2016), polynomial chaos expansion (PCE) (Hu and Youn, 2011; He et al., 2020), support vector regression (SVR) (Feng et al., 2019; Roy et al., 2019), radial basis function (RBF) (Li et al., 2018), Kriging (also called Gaussian process) (Kaymaz, 2005; Su et al., 2017; Zhou and Peng, 2020) and artificial neural network (ANN) (Cheng and Li, 2008; Ren et al., 2022). Accurate failure probability estimation by these models necessitates precise classification of samples as failing or non-failing, particularly near the limit state boundary. Therefore, various active learning strategies have been proposed to select samples adaptively and update the surrogate model efficiently. Efficient global reliability analysis (EGRA) (Bichon et al., 2008), active Kriging Monte Carlo simulation (AK-MCS) (Echard et al., 2011), and importance sampling and Kriging reliability method (AK-IS) (Echard et al., 2013) are the most popular active learning methods. Based on these methods, numerous enhanced methodologies, such as error rate-based adaptive Kriging (REAK) (Wang and Shafieezadeh, 2019), adaptive Kriging oriented importance sampling (AKOIS) (Zhang et al., 2020), and the surrogate-model based active learning method (SM-ALM) (Hong et al., 2022), have been developed to achieve notable efficiency and accuracy for scenarios with multiple failure areas and low failure probabilities. However, for certain complex engineering challenges, such as aerodynamic simulations (Huan et al., 2019) and vehicle collision analyses (Wu et al., 2019), their computational intensity poses a significant challenge in acquiring sufficient high-fidelity samples for con-

structing accurate surrogate models, especially under limited simulation resources.

Multi-fidelity surrogate-based methods provide a feasible way to reduce the computational cost of these reliability analysis problems. Although some low-fidelity models may have significant errors (e.g., simplified physical and coarse mesh models), low-fidelity samples can still provide some useful information, such as the changing trend of the response (Forrester et al., 2007; Guo et al., 2022). Consequently, it is crucial for multi-fidelity modeling to effectively capture the relationship between high-fidelity and low-fidelity responses. In recent years, a variety of multi-fidelity modeling approaches, including co-Kriging (Forrester et al., 2007), the nonlinear autoregressive scheme (Perdikaris et al., 2017), and multi-fidelity deep Gaussian processes (MF-DGP) scheme (Cutajar et al., 2019), have been developed. However, compared to active learning-based modeling methods, building a multi-fidelity model using a one-shot sampling strategy may significantly increase the computational cost due to the incomplete use of information. Thus, researchers are increasingly incorporating active learning into multi-fidelity scenarios, leveraging the benefits of multi-fidelity modeling while adaptively selecting new samples near failure domains for continuous model enhancement. For instance, Chaudhuri et al. (2019) proposed a multi-fidelity efficient global reliability analysis (mfEGRA) approach that combines the EGRA method with the multi-information source optimization method. To enhance the applicability of co-Kriging modeling in predicting the limit state function for reliability analysis, Liu et al. (2021) developed an extended expected improvement (EEI) infill criterion. Yi et al. (2020) proposed a learning function called the augmented expected feasibility (AEF) function for multi-fidelity modeling to reduce the computational burden of reliability analysis. To effectively capture the correlations between data with different fidelities, nested samples are commonly used to build surrogate models (Meng and Karniadakis, 2020; Chen et al., 2022). This leads to a huge number of low-fidelity samples. Besides, existing multi-fidelity surrogate-based modeling methods often use a scaling factor and an error term to represent the relationship between different fidelity samples. However, the scaling factor and error term

cannot completely consider possible nonlinear relationships, which may lead to an incorrect trend and unreliable predictions.

In this paper, we present a multi-fidelity surrogate modeling scheme combined with active learning to attain efficient reliability analysis with high accuracy. The primary research developments concern the following three aspects: (1) To improve the model's ability to represent the relationship between information with different fidelities, we introduce the nonlinear autoregressive scheme (Perdikaris et al., 2017) and construct a multi-fidelity surrogate named the nonlinear autoregressive multi-fidelity Kriging (NAMK) model. (2) In the process of model refinement, the traditional learning function is replaced by a collective multi-fidelity learning function, which selects new sampling points from the multi-fidelity sample space by comprehensively considering the sampling cost and the correlation between multi-fidelity samples. (3) To further reduce the number of samples, instead of directly sampling, nested low-fidelity samples are generated using a constructed residual model when selecting high-fidelity samples.

The remainder of the paper is organized as follows. A brief review of the basic theory of the proposed approach is given in Section 2. Section 3 introduces the proposed method in detail. Three numerical examples and an engineering case are provided in Section 4 to show the applicability of the proposed method. Conclusions are summarized in Section 5.

2 Foundational concepts

2.1 Kriging model

A Kriging model leverages the information from multiple samples to fit the original model, thereby enabling the estimation of responses and quantification of uncertainties for any given sampling points (Krige, 1951). A Kriging model can be formulated by

$$\hat{g}(\mathbf{x}) = \mathbf{h}(\mathbf{x})^T \boldsymbol{\beta} + Z(\mathbf{x}), \quad (2)$$

where $\mathbf{h}(\mathbf{x}) = [\mathbf{h}_1(\mathbf{x}), \dots, \mathbf{h}_k(\mathbf{x})]$ is the basis function, $\boldsymbol{\beta} = [\boldsymbol{\beta}_1, \dots, \boldsymbol{\beta}_k]$ is the vector of regression coefficients,

and $Z(\mathbf{x})$ is a Gaussian process characterized by a zero mean and a covariance

$$\text{Cov}[Z(\mathbf{a}), Z(\mathbf{b})] = \sigma_z^2 K(\mathbf{a}, \mathbf{b}), \quad (3)$$

where σ_z^2 denotes the variance of $Z(\mathbf{x})$; $K(\mathbf{a}, \mathbf{b})$ represents the correlation function and can be commonly defined as multiple forms. The Gaussian correlation function was used in this study because of its robustness and suitability (Jones et al., 1998). For an unknown point \mathbf{x}^* , its predicted value $\hat{G}(\mathbf{x}^*)$ and variance $\hat{\sigma}_G^2(\mathbf{x}^*)$ are expressed as

$$\hat{G}(\mathbf{x}^*) = \hat{\boldsymbol{\beta}} + \mathbf{r}^T(\mathbf{x}^*) \mathbf{K}^{-1}(\mathbf{Y} - \hat{\boldsymbol{\beta}} \mathbf{1}), \quad (4)$$

$$\hat{\sigma}_G^2(\mathbf{x}^*) = \sigma_z^2 \left(1 + \mathbf{u}^T (\mathbf{1}^T \mathbf{K}^{-1} \mathbf{1})^{-1} \mathbf{u} - \mathbf{r}^T(\mathbf{x}^*) \mathbf{K}^{-1} \mathbf{r}(\mathbf{x}^*) \right), \quad (5)$$

where $\mathbf{r}^T(\mathbf{x}^*) = [K(\mathbf{x}^*, \mathbf{x}^{(1)}), \dots, K(\mathbf{x}^*, \mathbf{x}^{(n)})]^T$, and $\mathbf{u} = \mathbf{1}^T \mathbf{K}^{-1} \mathbf{r}^T(\mathbf{x}^*) - 1$.

2.2 Multi-fidelity modeling method

The objective of the multi-fidelity modeling method is to establish a mapping relationship between low-fidelity and high-fidelity responses by creating a joint model that integrates multi-source information (Kennedy and O'Hagan, 2000; Le and Garnier, 2014). In our research, we used a nonlinear autoregressive scheme (Perdikaris et al., 2017) to capture the relationship between multi-fidelity data because of its excellent nonlinear characterization performance. The nonlinear autoregressive scheme constructs a nested input structure by incorporating the response of low-fidelity samples into the input of the high-fidelity model. Compared with the MF-DGP scheme (Cutajar et al., 2019), the nonlinear autoregressive scheme trains each fidelity level model independently, resulting in low computational complexity and flexible modeling.

Suppose there are sample sets $D_m = [\mathbf{X}_m, \mathbf{Y}_m]$, $m = 1, \dots, H$ with increasing fidelity m . The nonlinear autoregressive multi-fidelity model is given by

$$g_m(\mathbf{x}) = Q_m([\mathbf{x}, g_{m-1}(\mathbf{x})]), \quad (6)$$

where $g_m(\mathbf{x})$ is the surrogate model constructed by the samples with fidelity level m , and $Q_m \sim \text{GP}(g_m | \mathbf{0}, \mathbf{r}_m((\mathbf{x}, g_{m-1}(\mathbf{x})), (\mathbf{x}^\top, g_{m-1}(\mathbf{x}^\top))); \boldsymbol{\theta}_m)$. $Q_m(\cdot)$ can more fully represent the relationship between samples with different fidelities, and its covariance kernel is given by

$$\begin{aligned} K_{m_g} &= K_{m_p}(\mathbf{x}, \mathbf{x}^\top; \boldsymbol{\theta}_{m_p}) \\ &\times K_{m_r}(g_{m-1}(\mathbf{x}), g_{m-1}(\mathbf{x}^\top); \boldsymbol{\theta}_{m_r}) \\ &+ K_{m_s}(\mathbf{x}, \mathbf{x}^\top; \boldsymbol{\theta}_{m_s}), \end{aligned} \quad (7)$$

where K_{m_p} , K_{m_r} and K_{m_s} are covariance functions and $\boldsymbol{\theta}_m = [\boldsymbol{\theta}_{m_p}, \boldsymbol{\theta}_{m_r}, \boldsymbol{\theta}_{m_s}]$ express their hyperparameters.

3 Proposed method

In this section, the surrogate-based reliability framework using a NAMK model and active learning is presented. The core strategy involves establishing a NAMK model using the nonlinear autoregressive scheme, followed by iterative refinement based on adaptively selected new samples. Firstly, initial multi-fidelity samples are selected in the specified parameter range and an initial surrogate model is constructed using NAMK. In the process of model updating, the position and fidelity of new samples are determined by a collective learning function. Once a high-fidelity sample is determined, a corresponding nested low-fidelity sample can be automatically generated according to a residual model. Finally, a stopping criterion using relative error estimation terminates the active learning process. Figure 1 shows a flowchart of the approach.

3.1 Initial samples selection

The distribution of initial samples largely determines the performance of the surrogate model and the efficiency of the active learning process. When the initial samples are evenly filled in the design space, a comprehensive evaluation of the limit state function can be obtained. A Latin hypercube sampling method based on evolutionary operation (EVOP-LHS) (For-

rester et al., 2008) is used to obtain initial low-fidelity samples $\{\mathbf{X}_m\}_{m=1}$ that are evenly distributed in the sample space. Then, an exchange algorithm (Reisenthel and Allen, 2014) is adopted to obtain the higher fidelity samples $\{\mathbf{X}_m\}_{m=2,\dots,H}$ to ensure the nesting property and distribution uniformity among samples with different fidelities.

3.2 Construction of the residual model and generation of the nested low-fidelity sample

In the case of a multi-fidelity surrogate model, when a nested relationship exists between training samples of different fidelity levels, the model can provide a more precise description of the relationship between the samples (Perdikaris et al., 2017; Liu et al., 2020). This nested relationship allows the model to capture the intricate connections and dependencies among the samples with greater accuracy. The nested relationship between training samples when \mathbf{x} is one dimensional is presented in Fig. 2a. However, extra calculations are needed to obtain nested low-fidelity samples in the process of model updating (Fig. 2b).

In this study, a residual modeling method was used to generate nested low-fidelity samples. The core idea of residual modeling is to capture the discrepancy between the high-fidelity sample response values Y_m and the low-fidelity sample response values Y_{m-1} by constructing a residual model $F_{\text{Re}}(\cdot)$, and then calculate the response of nested low-fidelity samples. The detailed construction process of the residual model can be found in the electronic supplementary materials (Section S1).

3.3 Construction of the NAMK model and calculation of the predicted response value

The main goal of the multi-fidelity modeling strategy is to use nested multi-fidelity training samples $[\mathbf{X}_m, Y_m]_{m=1,\dots,H}$ to capture the relationship $q_m(\cdot)$ between $g_m(\mathbf{x})$ and $g_{m-1}(\mathbf{x})$. In this study, the nonlinear autoregressive scheme (Perdikaris et al., 2017) was used to establish a multi-fidelity surrogate model in combination with a Kriging model since it can effectively capture the nonlinear relationship between different fidelity information by incorporating an additional input into the high-fidelity model.

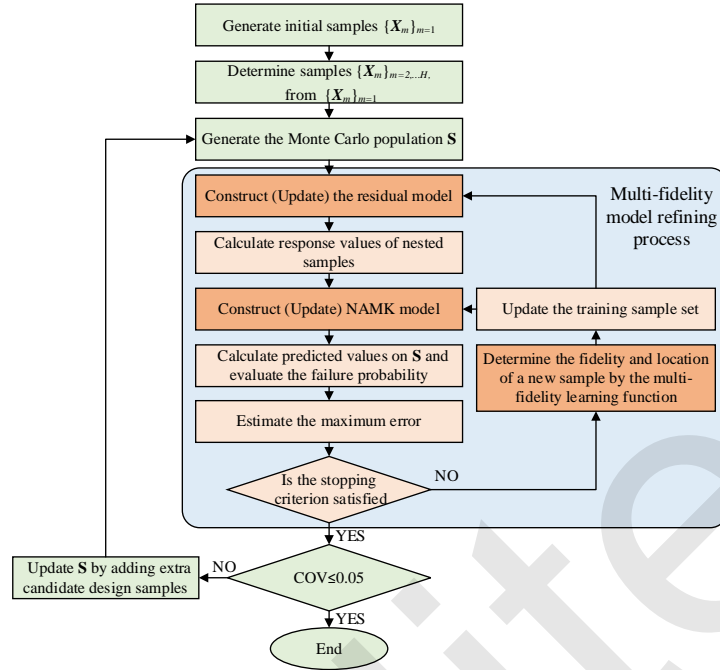


Fig. 1 Flowchart of the proposed approach

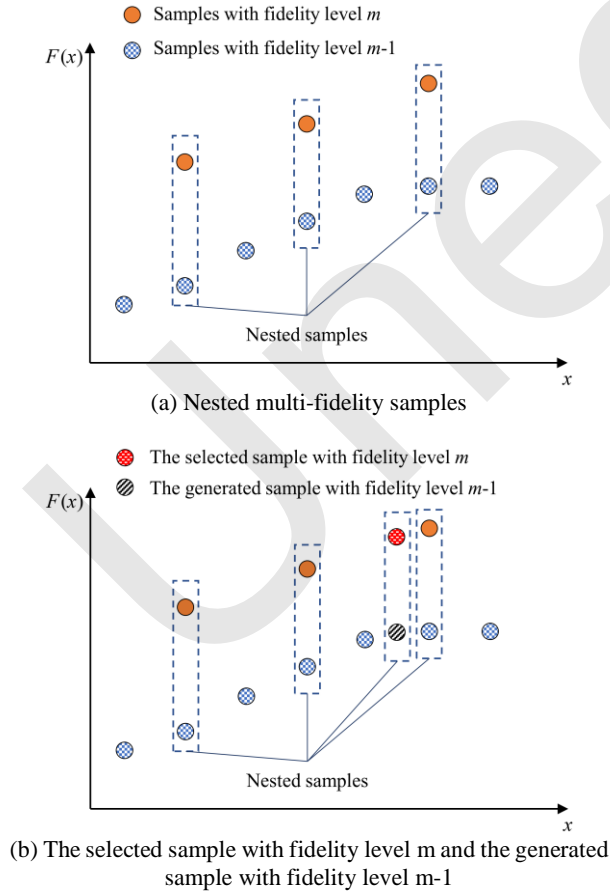


Fig. 2 Relationships between multi-fidelity samples

An initial Kriging model $Z_{m=1}(\cdot)$ was constructed using the lowest fidelity sample set $[X_m, Y_m]_{m=1}$. After the sample set $[X_m, Y_m]_{m=2}$ of the higher fidelity level and predicted response values $\hat{G}_{m=1}(X_{m=1})$ are obtained, $Z_{m=2}(\cdot)$ is built by

$$Y_{m=2} = Z_{m=2}(X_{m=2}, \hat{G}_{m=1}(X_{m=1})). \quad (8)$$

From Eq. (8), it is known that $Z_{m=2}(\cdot)$ can not only accurately predict the response values $X_{m=1}$, but also characterize the relationship between samples with fidelity $m=1$ and $m=2$.

Once $Z_{m=H}(\cdot)$ is determined using the highest fidelity sample set $[X_m, Y_m]_{m=H}$ and $\hat{G}(X_{m=H-1})$, the NAMK model $V_{m=H}(\cdot)$ is formulated by an autoregressive form

$$V_{m=H}(x) = \begin{cases} Z_{m=1}(x) \\ Z_{m=2}(x, \hat{G}_{m=1}(x)) \\ \dots \\ Z_{m=H}(x, \hat{G}_{m=H-1}(x)). \end{cases} \quad (9)$$

Predictive response values $\hat{G}_m(\mathbf{x}_i)$ of candidate samples can be calculated according to $V_{m=H}(\cdot)$, namely

$$\hat{G}_m(\mathbf{x}_i) = Z_m(\mathbf{x}_i, \hat{G}_{m-1}(\mathbf{x}_i)), m = 2, \dots, H \quad (10)$$

where $\mathbf{x}_i, i = 1, \dots, N_{\text{MCS}}$ are candidate samples from Monte Carlo population \mathbf{S} .

3.4 Active learning strategy

3.4.1 Determination of new samples

A traditional learning function usually selects useful samples according to the posterior mean and standard deviation of candidate training samples, and is applicable only for active learning problems with a single information source scenario. For multi-source information, the site and fidelity of samples should be determined in the active learning process. In addition, models with different fidelity have different calculation costs, so the sampling cost also needs to be considered in the process of selecting new samples. Therefore, a new collective multi-fidelity learning function consisting of three parts is proposed to select suitable samples. The formulation of this learning function is

$$F_{\text{MF}}(\mathbf{x}, m) = U_{\text{MF}}(\mathbf{x}) \times C_{\text{R}}(\mathbf{x}, m) \times \frac{1}{c(m)}, m = 1, \dots, H \quad (11)$$

in which, $c(m)$ is the function of sampling cost, which is used to assess the relative computational cost associated with samples of different fidelities, and is usually expressed as

$$c(m) = \frac{T(m)}{T(H)}, m = 1, \dots, H \quad (12)$$

where $T(\cdot)$ represents the calculation time required to obtain the sample response; $U_{\text{MF}}(\mathbf{x})$ represents the expected feasibility of candidate points under different fidelities. Its function can be obtained by extending U-learning function (Echard et al., 2011), i.e.,

$$U_{\text{MF}}(\mathbf{x}) = \frac{\sigma_{\hat{G}_m}(\mathbf{x})}{|\hat{G}_H(\mathbf{x})|}, m = 1, \dots, H \quad (13)$$

where $\sigma_{\hat{G}_m}(\mathbf{x})$ represents the posterior standard deviation of samples with fidelity level m , and $\hat{G}_H(\mathbf{x})$ is the response of the highest fidelity model corresponding to the current sample. Using $U_{\text{MF}}(\mathbf{x})$, these candidates, which are characterized by their proximity to the high-fidelity limit state function and high uncertainty, can be effectively identified and selected. $C_{\text{R}}(\mathbf{x}, m)$ represents the relative correlation of multi-fidelity samples, which depends mainly on the predicted response and posterior variance (Reisenthel and Allen, 2014). It can be denoted as

$$C_{\text{R}}(\mathbf{x}, m) = \frac{\sigma_{\hat{G}_m}(\mathbf{x})}{|\hat{G}_H(\mathbf{x}) - \hat{G}_m(\mathbf{x})| + \sigma_{\hat{G}_H}(\mathbf{x})}, \quad (14)$$

where $\sigma_{\hat{G}_H}(\mathbf{x})$ is larger than $\sigma_{\hat{G}_m}(\mathbf{x})$ because the uncertainty is transmitted along each recursive step. When $m \geq 2$, the predicted variance of $\sigma_{\hat{G}_m}(\mathbf{x})$ can be obtained through

$$p(\hat{G}_m(\mathbf{x})) = \int p(\mathbf{x}, \hat{G}_{m-1}(\mathbf{x})) p(\hat{G}_{m-1}(\mathbf{x})) d\mathbf{x}, \quad (15)$$

where $p(\hat{G}_{m-1}(\mathbf{x}))$ is the posterior distribution of the previous fidelity level and $\sigma_{\hat{G}_m}(\mathbf{x})$ is obtained by calculating its confidence interval. To alleviate the computational burden associated with computing Monte Carlo integrals for all candidate samples, $\sigma_{\hat{G}_m}(\mathbf{x})$ is estimated as

$$\sigma_{\hat{G}_m}(\mathbf{x}) = \sum_{q=1}^m \sigma_{\hat{G}}^{(q)}(\mathbf{x}), \quad (16)$$

where $\sigma_{\hat{G}}^{(q)}(\cdot)$ is the standard deviation of the Kriging model when the fidelity level is equal to q . $C_{\text{R}}(\mathbf{x}, m)$ is applied to characterize the acceptance of low-fidelity samples. When $m = H$, $C_{\text{R}}(\mathbf{x}, m)$ is equal to 1.

3.4.2 Stopping criterion

A conservative stopping criterion can result in unnecessary evaluations of the expensive limit state function, whereas premature termination of the sampling process may lead to incorrect estimation of the failure probability. To achieve fast convergence, the efficient error-based stopping criterion (ESC) (Wang and Shafieezadeh, 2019) was extended for use in multi-source information scenarios. Based on the upper limit of the relative error, the error-based stopping criterion is defined as

$$\begin{aligned} \varepsilon &= \left| \frac{\hat{N}_f}{N_f} - 1 \right| \\ &\leq \max \left(\left| \frac{\hat{N}_f}{\hat{N}_f - \hat{S}_f^u} - 1 \right|, \left| \frac{\hat{N}_f}{\hat{N}_f + \hat{S}_s^u} - 1 \right| \right) = \hat{\varepsilon}_{\max}, \end{aligned} \quad (17)$$

where N_f and \hat{N}_f denote the number of real and estimated failure samples, respectively; \hat{S}_f^u and \hat{S}_s^u are the upper bound of the confidence interval of \hat{S}_f and \hat{S}_s , respectively; $\hat{\varepsilon}_{\max}$ is the specified threshold, whose detailed calculation process can be found in the supplementary materials (Section S2).

3.5 Steps of the proposed method

The details of application steps are as follows:

Step 1: Generate initial samples $\{\mathbf{X}_m\}_{m=1}^H$ by EVOP-LHS, and select samples $\{\mathbf{X}_m\}_{m=2, \dots, H}$ by the exchange algorithm (Forrester et al., 2007).

Step 2: Generate the Monte Carlo population \mathbf{S} according to the statistical characteristics of the design variables.

Step 3: Construct (Update) the residual model $F_{\text{Re}}(\cdot)$ according to current samples with different fidelity and their response values.

Step 4: Calculate response values of nested samples based on $F_{\text{Re}}(\cdot)$.

Step 5: Construct (Update) the NAMK model using current samples with different fidelity and their response values.

Step 6: Calculate the predicted values using the constructed NAMK model, and estimate the failure

probability by $\hat{p}_f = \frac{1}{N_{\text{MCS}}} \sum_{i=1}^{N_{\text{MCS}}} I(\hat{G}_H(\mathbf{x}_i))$, where $I(\hat{G}_H(\mathbf{x}_i)) = 0$ when $\hat{G}_H(\mathbf{x}_i) > 0$, $I(\hat{G}_H(\mathbf{x}_i)) = 1$ when $\hat{G}_H(\mathbf{x}_i) \leq 0$.

Step 7: Estimate the maximum error according to \mathbf{S} .

Step 8: Check the stopping criterion. If the stopping condition is met, proceed to Step 10; otherwise, return to Step 9.

Step 9: Determine the location and fidelity of the new sample by $\{\mathbf{x}^{\text{new}}, m^{\text{new}}\} = \arg \max_{\mathbf{x}, m} (F_{\text{MF}}(\mathbf{x}, m))$, and

update the training sample set.

Step 10: Check the coefficient of variation by

$$\text{COV} = \sqrt{\frac{1 - \hat{p}_f}{N_{\text{MCS}} \hat{p}_f}}. \text{ If } \text{COV} \leq 0.05, \text{ turn to Step 12;}$$

otherwise, return to Step 11.

Step 11: Update \mathbf{S} by adding extra candidate samples, and turn to Step 2.

Step 12: Report \hat{p}_f .

4 Case studies

To assess the accuracy and efficiency of the proposed approach, we investigated three numerical cases of variable complexity, as well as an engineering case. The code was implemented in MATLAB, and the Kriging model was constructed using the DACE toolbox (Lophaven et al., 2002). Several state-of-the-art methods for reliability analysis methods based on surrogate modeling were adopted for comparison: (1) EGRA (Bichon et al., 2008), (2) AK-MCS+U (Echard et al., 2013), (3) REAK (Wang and Shafieezadeh, 2019), (4) AKOIS (Zhang et al., 2020), (5) mfEGRA (Chaudhuri et al., 2021), and (6) AMK-MCS+AEFF (Liu et al., 2020). The efficiency of these methods was compared in terms of the average cost considering all fidelity samples, and their accuracy was quantified using the average relative error of failure probability, which can be characterized as

$$\eta = \frac{1}{n_r} \sum_i^{n_r} |p_f^{\text{MCS}} - \hat{p}_f|, \quad (18)$$

where n_i is the number of repeated calculations. To achieve a robust result, all methods were performed 10 times for each case.

4.1 Example 1: multimodal function

In this example, the multimodal function (Bichon et al., 2008), a classical test function in the field of reliability, was used to demonstrate the active learning process in detail and assess the effectiveness of the proposed method. The high-fidelity model of the limit state function is defined by

$$f_3(\mathbf{x}) = 2 - \frac{(x_1^2 + 4)(x_2 - 1)}{20} - \sin\left(\frac{5x_1}{2}\right), \quad (19)$$

where x_1 and x_2 are normally distributed with a mean value of $[1.5, 2.5]$ and a variance of $[1, 1]$. The two low-fidelity models (Chaudhuri et al., 2021) were represented as

$$f_2(\mathbf{x}) = f_3(\mathbf{x}) + \sin\left(\frac{5x_1}{22} + \frac{5x_2}{44} + \frac{5}{4}\right), \quad (20)$$

$$f_1(\mathbf{x}) = f_3(\mathbf{x}) + 3\sin\left(\frac{5x_1}{11} + \frac{5x_2}{11} + \frac{35}{11}\right). \quad (21)$$

Assume that the cost of each fidelity model remains the same throughout the domain. The costs are $c(3)=1$, $c(2)=0.1$, and $c(1)=0.01$, respectively (Marques et al., 2018). The contour plots of three fidelity models in the demonstration case and the limit state function of each model are shown in Fig. 3.

Figure 4 shows several iterations of the random running sequential process of the proposed scheme.

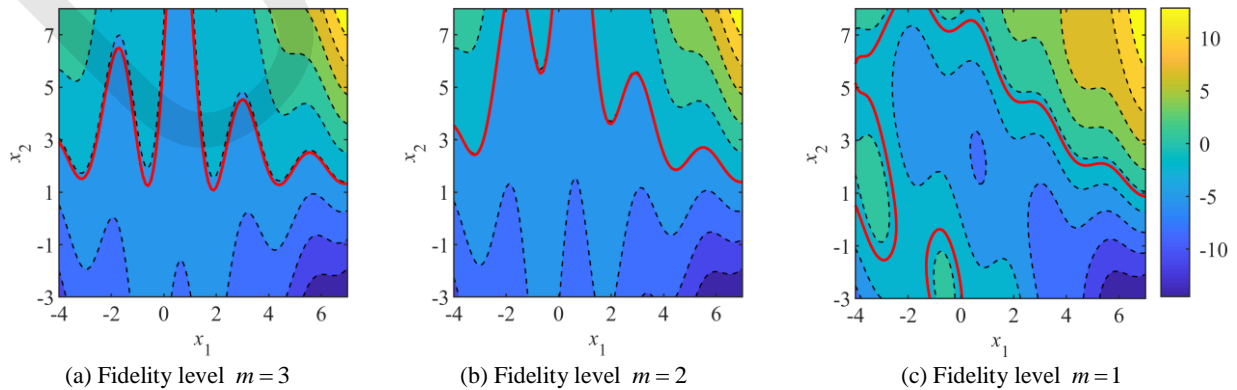


Fig. 3 Contours of $f_m(\mathbf{x})$ using the three fidelity models for the multimodal function (solid red lines represent the limit state plane)

Figure 4a depicts the position of the initial samples with variable fidelity. The proposed method firstly generates 24 samples with fidelity level $m=1$ from the design space $[\mu-5\sigma, \mu+5\sigma]$ by EVOP-LHS and then selects 12 samples with fidelity level $m=2$ and 6 samples with fidelity level $m=3$ by the exchange algorithm. Figures 4b-4e show the process of selecting new samples, generating nested samples and the iterative process of the contour. As illustrated in Figs. 4b and 4c, the proposed method tends to prioritize the selection of low-fidelity samples in the initial iterations due to the limited knowledge of the limit state. This cautious approach allows for a broader exploration of the design space and facilitates the acquisition of crucial information about the system's behavior. However, as understanding of the limit state deepens, the method gradually shifts towards selecting high-fidelity samples in the later iterations, as observed in Figs. 4d and 4e. This adaptive sampling strategy allows the method to focus on areas of higher uncertainty and refine the surrogate model for more accurate predictions. In addition, because of the $U_{MF}(\mathbf{x})$, the points explored in the active learning process are concentrated mainly near the limit state, which is conducive to more accurate evaluation of the failure probability. Consequently, the limit state plane evaluated by the NAMK model accurately tracks the actual failure boundary (Fig. 4e). The performance of the proposed approach was compared with MCS, EGRA, AK-MCS+U, REAK, AKOIS, mfEGRA, and AMK-MCS+AEFF. The results of these comparisons are summarized in Table 1.

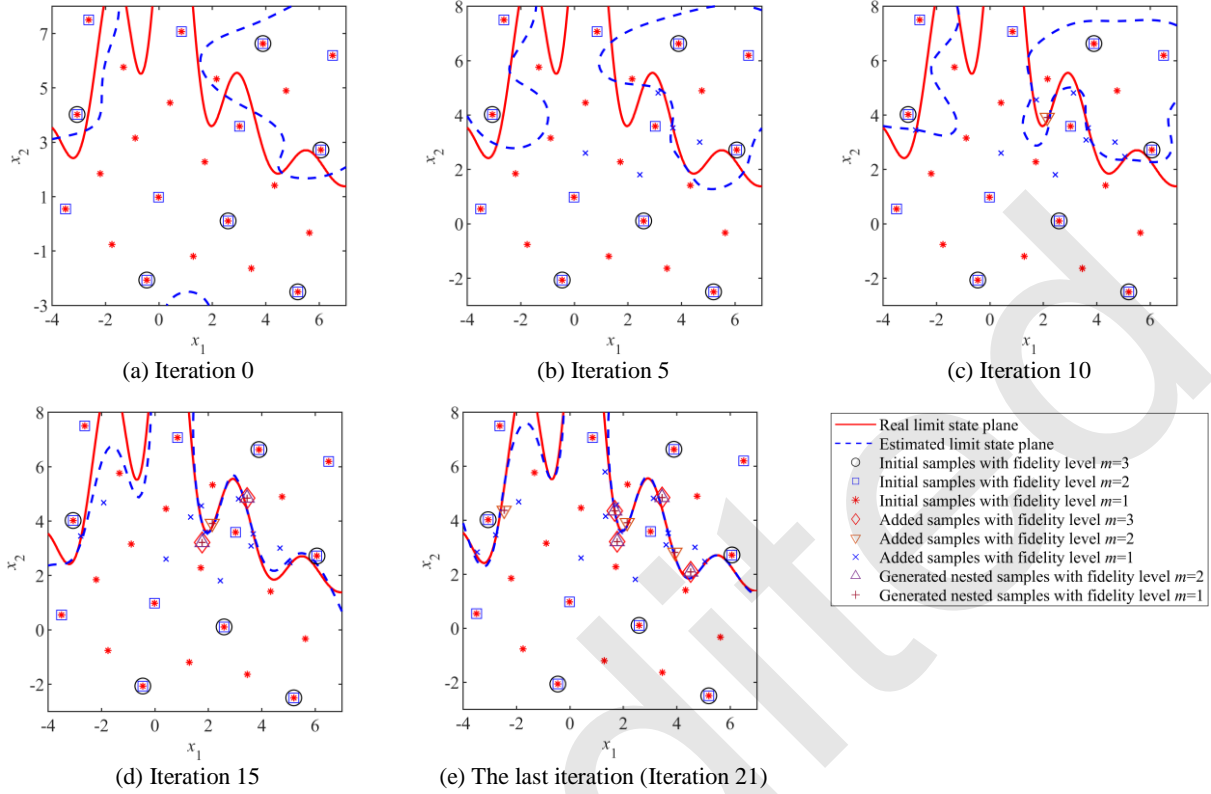


Fig. 4 The iteration process of the proposed method on the multimodal function

Table 1 Results of different methods for the multimodal function

Methods	Cost	$\hat{p}_f (\times 10^{-2})$	COV (%)	Error (%)
MCS	10^6	3.13	0.56	-
EGRA	49.3	3.14	3.93	0.24
AK-MCS+U	39.2	3.13	3.93	2.84×10^{-2}
REAK	28.6	3.14	3.92	0.74
AKOIS	30.8	3.16	3.90	1.13
mfEGRA	15.24(12.1+26.6×0.1+47.9×0.01)	3.09	3.96	1.45
AMK-MCS+AEFF	14.9(10.3+46×0.1)	3.12	3.93	1.15
Proposed method	12.90(10.9+16.1×0.1+39.2×0.01)	3.12	3.89	0.97

As listed in Table 1, the cost of the proposed method was 12.90, which was the lowest among all methods. The relative error of the proposed method was only 0.97%, which was smaller than those of AKOIS, mfEGRA, and AMK-MCS+AEFF. The method’s relative error was merely 0.97%, outperforming AKOIS, mfEGRA, and AMK-MCS+AEFF in accuracy. Notably, while AK-MCS+U achieved high accuracy, its computational cost of 39.2 was 3.04 times higher than that of our method. Compared to single-fidelity active learning methods such as EGRA and REAK, our method significantly reduced the cost

while maintaining similar accuracy levels. To further prove the robustness of the proposed method, Fig. 5 shows boxplots of all the listed methods in terms of total cost and relative error. Our proposed method showed good stability in both efficiency and accuracy due to the use of the error-based stopping criterion.

4.2 Example 2: 4-D PARK function

For the second example, we used the 4-D PARK function (Cutajar et al., 2019) to validate the effectiveness of the proposed method in highly nonlinear problems. The 4-D PARK function can be expressed

as

$$f_2(\mathbf{x}) = \frac{x_1}{2} \left[\sqrt{(x_2 + x_3^2) \frac{x_4}{x_1^2} + 1} - 1 \right] + (x_1 + 3x_4) \exp[\sin(x_3) + 1] - 2, \quad (22)$$

$$f_1(\mathbf{x}) = \left[\frac{\sin(x_1)}{10} + 1 \right] f_2(\mathbf{x}) + x_2^2 + x_3^2 - 2x_1 + 0.5, \quad (23)$$

where $f_2(\mathbf{x})$ is the high-fidelity model, and $f_1(\mathbf{x})$ is the low-fidelity model, all inputs obey the uniform distribution of $[0, 1]$, and the costs are set to $c(2)=1$ and $c(1)=0.1$, respectively. The running results of the different methods applied to this example are shown in Table 2.

Table 2 shows that our proposed method effectively leverages multi-fidelity samples to establish a precise mapping between low-fidelity and high-fidelity samples, thereby significantly reducing computational overhead and delivering accurate failure probability estimates. In terms of efficiency, our method surpassed all others, incurring a calculation cost of only 28.70. Regarding accuracy, while the calculation error of our method was marginally higher than those of AK-MCS+U, REAK, and AKOIS, its computational cost was 48.0%, 67.1%, and 60.7% lower, respectively. Furthermore, due to the pronounced nonlinear relationship between the high-fidelity and low-fidelity models, mfRGRA and AK-MCS+U failed to achieve satisfactory accuracy, highlighting the importance of accurately capturing the nonlinear relationship in multi-fidelity modeling.

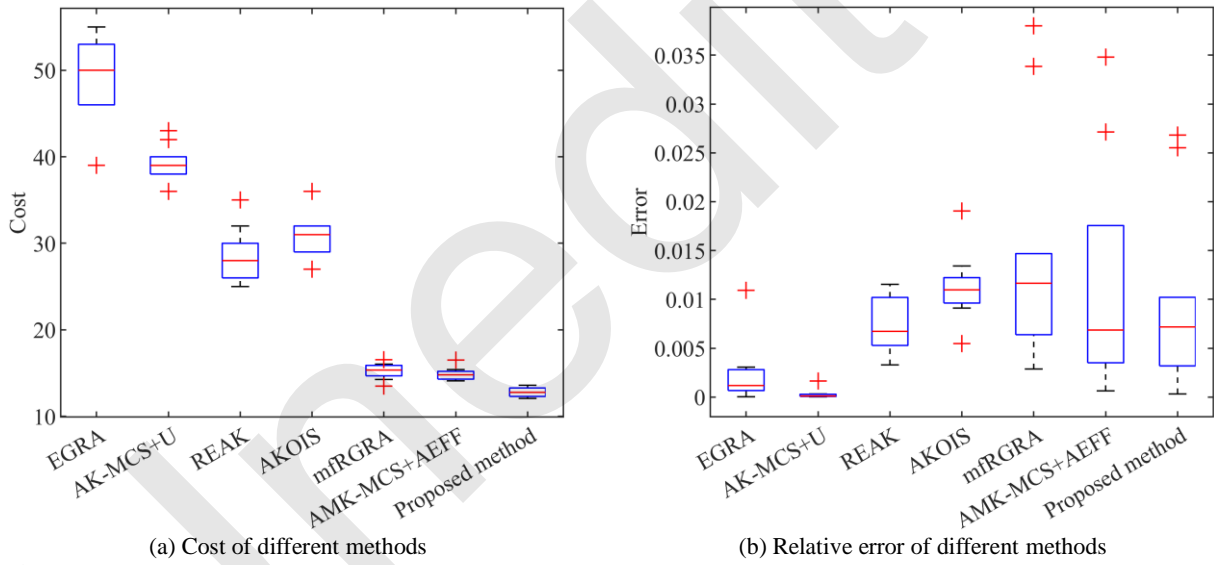


Fig. 5 Boxplots of cost and relative error of different methods

Table 2 Results of different methods for the 4-D PARK function

Methods	Cost	$\hat{p}_f (\times 10^{-2})$	COV (%)	Error (%)
MCS	1×10^6	3.86	0.50	-
EGRA	72.2	3.92	3.50	2.01
AK-MCS+U	59.8	3.86	3.52	0.13
REAK	42.8	3.87	3.52	0.36
AKOIS	47.3	3.84	3.54	0.48
mfEGRA	40.15(30.6+95.5×0.1)	3.73	3.60	5.80
AMK-MCS+AEFF	38.71(29.8+89.1×0.1)	3.81	3.55	2.13
Proposed method	28.70(22.5+62.0×0.1)	3.85	3.54	0.51

4.3 Example 3: vehicle side impact problem

In this section, we assess the accuracy and efficiency of the proposed scheme in tackling complex problems by using the vehicle side impact problem (Youn et al., 2004 and Yi et al., 2021) as a case study. This problem is characterized by a 7-dimensional limit state function, which can be represented as

$$f_2(\mathbf{x}) = 0.489x_1x_4 + 0.843x_2x_3 - 0.0432x_5x_6 + 0.0556x_5x_7 + 0.00078x_7^2 - 0.75, \quad (24)$$

$$f_1(\mathbf{x}) = f_2(\mathbf{x}) - \frac{1}{10} \left(0.489(x_1 - 0.1)(x_4 - 0.1) + 0.843(x_2 - 0.1)(x_3 - 0.1) + 0.0432(x_2 - 0.1)(x_3 - 0.1) + 0.0556(x_5 - 0.1)(x_7 - 0.1) + 0.00078(x_7 - 1) \right), \quad (25)$$

where $f_2(\mathbf{x})$ is the high-fidelity model, and $f_1(\mathbf{x})$

is the low-fidelity model. The statistical characteristics of \mathbf{x} are shown in Table 3, and the costs were set to $c(2)=1$ and $c(1)=0.05$ (Yi, et al., 2021), respectively. Table 4 summarizes the running results of different methods applied to this problem.

Table 4 shows that, compared to other single-fidelity active learning methods, the calculation error of our proposed method was 1.19%, slightly exceeding that of AK-MCS+U, REAK, and AKOIS, but its cost was obviously reduced. Furthermore, owing to the NAMK model's efficient capture of the nonlinear relationship between multi-fidelity samples, our method outperformed other multi-fidelity modeling methods, including mfEGRA and AMK-MCS+AEFF, in both computational cost and efficiency. Figure 6 provides a comparison of the convergence of the relative error of failure probability for the different methods. Our proposed method achieved a lower relative error level with a relatively small number of calculations, indicating its superior convergence performance in this case.

Table 3 Distributions and parameters of \mathbf{x} of the vehicle side impact problem

Variables	Mean	Standard deviation	Distribution	Description
x_1	1.38	0.3	Normal	Floor side inner
x_2	1.38	0.3	Normal	Door beam
x_3	1.38	0.3	Normal	Door beltline
x_4	1.38	0.3	Normal	Roof rail
x_5	0.3	0.06	Normal	Floor side inner
x_6	0	10	Normal	Barrier height
x_7	0	10	Normal	Barrier hitting

Table 4 Results of different methods for the vehicle side impact problem

Methods	Cost	$\hat{p}_f (\times 10^{-4})$	COV (%)	Error (%)
MCS	5×10^6	1.64	3.49	-
EGRA	79.9	1.74	3.39	6.86
AK-MCS+U	91.8	1.65	3.49	0.55
REAK	65.2	1.62	3.51	1.09
AKOIS	58.0	1.65	3.48	0.82
mfEGRA	53.9(48.4+109.3×0.05)	1.60	3.54	2.41
AMK-MCS+AEFF	49.5(42.6+137.2×0.05)	1.61	3.52	1.28
Proposed method	37.6(33.6+80.4×0.05)	1.67	3.48	1.19

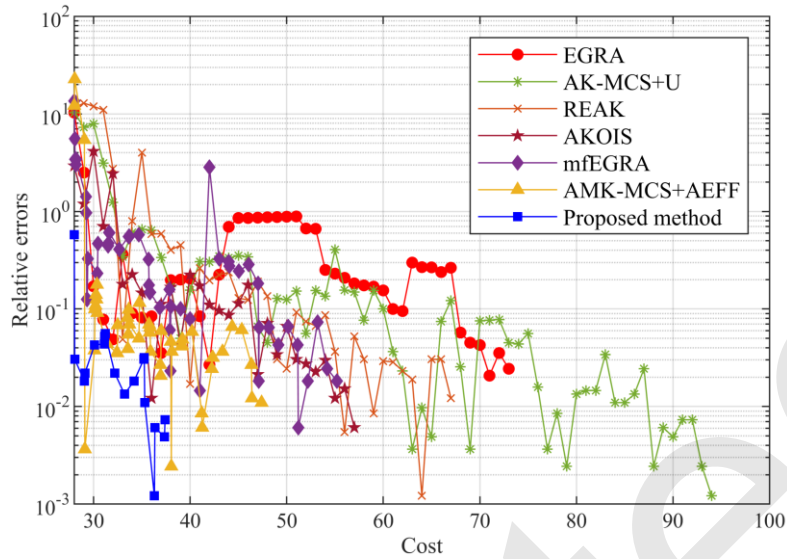
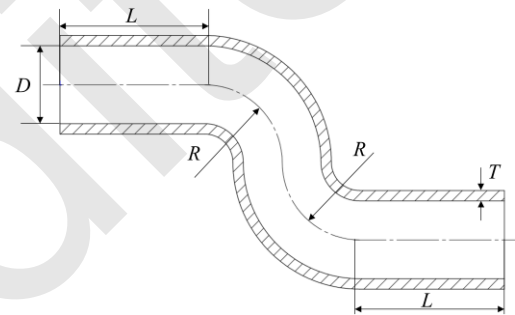


Fig. 6 Relative error of failure probability of different methods (shown in log-scale)

4.4 Engineering application: aircraft tubing

Tubing assembly is widely used in aircraft sub-systems (e.g., hydraulic systems, fuel systems, and environmental control systems) and significantly influences aircraft reliability and safety. In this case, we investigated the reliability analysis of the overall stability of aircraft tubing (Li and Wang, 2019) to demonstrate the practicality of the proposed method in engineering problems. The structural profile of the tubing is visually depicted in Fig. 7, illustrating its geometric configuration and layout. Additionally, Table 5 provides an overview of the statistical characteristics associated with the structural parameters relevant to the tubing. The tubing is constructed from steel material with a Poisson’s ratio of 0.27 and Young’s modulus of 200 GPa, and a pressure of $P = 33 \text{ Mpa}$ was applied to the inner surface. The critical threshold of failure was defined as a maximum total deformation of tubing greater than 0.01mm.



(b) Geometry of the aircraft tubing
Fig. 7 Aircraft tubing



(a) Aircraft fuel system

In this work, the finite element method (FEM) was used to obtain the maximum deformation of the tubing. In the analysis of the tubing assembly, two different mesh configurations were used: a fine mesh and a coarse mesh. The solution obtained from the fine mesh was considered the high-fidelity model, which provided more accurate and detailed results. The solution obtained from the coarse mesh was regarded as the low-fidelity model, which provided approximate results with reduced computational cost. The commercial software ABAQUS was used to carry out the finite element analysis. For the high-fidelity model, a mesh consisting of 18,432 elements was used to ensure accurate results. Conversely, a mesh model with only 880 elements was used as the low-fidelity model to facilitate faster computations. The mesh of the high-fidelity model is depicted in Fig. 8a, while that of the low-fidelity model is shown in Fig. 8b.

Figure 9 illustrates the simulation results obtained from the different fidelity models. Similar displacement distributions in Figs. 9a and 9b indicate that using the low-fidelity model was a reasonable simplification method. Moreover, the high-fidelity and low-fidelity model simulation times were 17.2 s and 2.1 s, respectively. Therefore, the costs were set to $c(2)=1$ and $c(1)=1/8$, respectively. Table 6 presents the results of the different methods for reliability analysis of aircraft tubing.

From the results provided in Table 6, we conclude that our proposed method had the best efficiency among all the methods. In terms of the calculation error, the relative error of our proposed method was 1.07%, which was only slightly larger than that of AK-MCS+U and REAK, and their calculation costs were several times that of our proposed method. In summary, our proposed method showed excellent performance in this engineering application.

Table 5 Statistical characteristics of variables of the aircraft tubing

Variables	Meaning	Mean (mm)	Standard deviation (mm)	Distribution
D	Inner diameter	17	0.2	Normal
T	Thickness	2.98	0.05	Normal
R	Radius of bending	2.93	0.11	Lognormal
L	Length	3.56	0.012	Lognormal

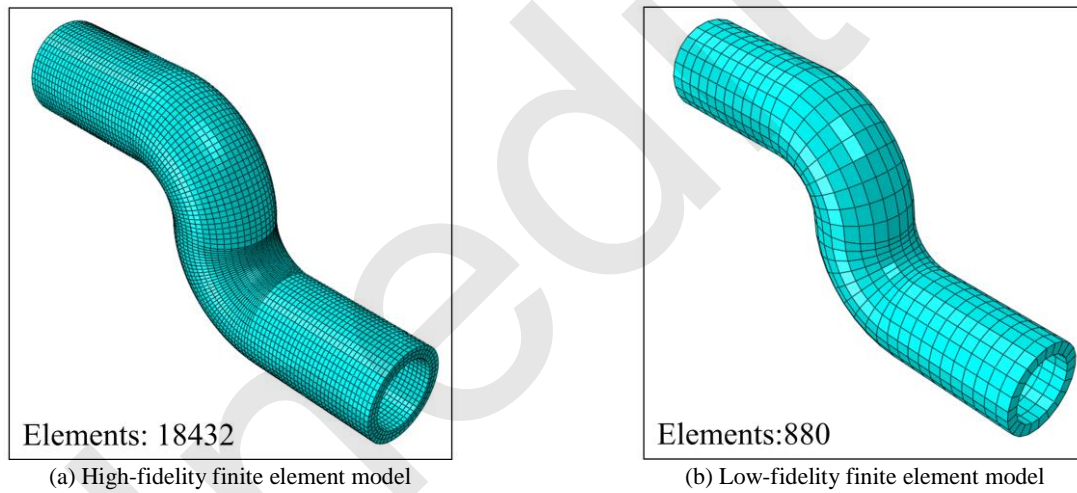


Fig. 8 The mesh grids of the high-fidelity model and low-fidelity model

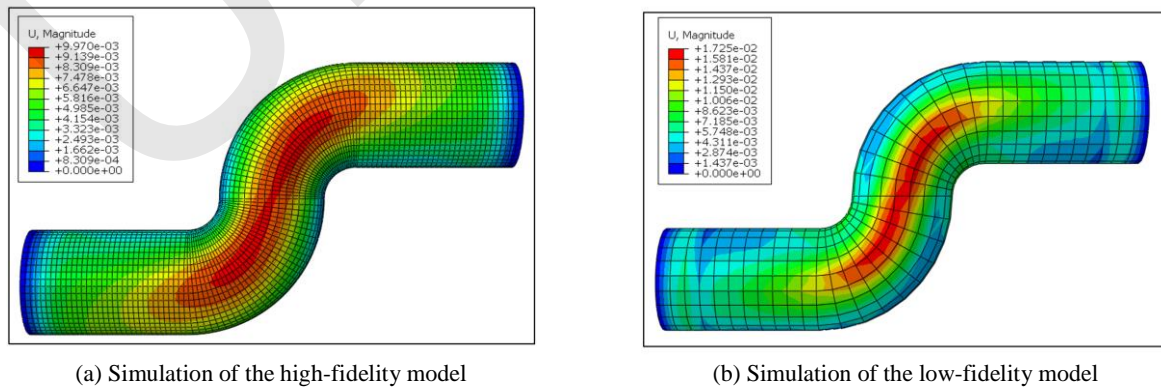


Fig. 9 The simulation results of the high-fidelity model and low-fidelity model

Table 6 Results of different methods for the aircraft tubing problem

Methods	Cost	$\hat{p}_f (\times 10^{-2})$	COV (%)	Error (%)
MCS	1×10^4	4.92	4.41	-
EGRA	43.9	4.72	4.51	5.09
AK-MCS+U	38.5	4.93	4.39	0.66
REAK	34.1	4.95	4.36	0.80
AKOIS	37.9	4.96	4.35	1.12
mfEGRA	26.2(20.6+44.8 \times 1/8)	4.87	4.64	2.10
AMK-MCS+AEFF	23.6(17.6+48.2 \times 1/8)	4.96	4.36	1.41
Proposed method	18.8(14.7+32.6 \times 1/8)	4.90	4.43	1.07

5 Conclusions

In this paper, we propose a novel nonlinear autoregressive multi-fidelity Kriging-based method with active learning for efficient and accurate reliability analysis. This method leverages NAMK modeling to accurately capture nonlinear relationships between multi-fidelity samples. This can improve the generalization performance of a surrogate model. A multi-fidelity learning function considering the correlation and sampling cost of various fidelity samples can adaptively determine the position and fidelity of the new sample. When a high-fidelity sample is selected by the learning function, the constructed residual model used to generate a nested low-fidelity sample reduces the calls of the low-fidelity model.

The performance of the proposed method was verified using three benchmark numerical examples of variable complexity, as well as an engineering example. Compared to EGRA, AK-MCS+U, REAK, and AKOIS, the proposed method showed effective use of multi-source information, resulting in a significant reduction in the number of high-fidelity samples while maintaining calculation accuracy. Additionally, the proposed method exhibited improved accuracy in capturing the nonlinear relationship between samples of different fidelity compared to mfEGRA and AMK-MCS+AEFF. Moreover, during the model updating process, the proposed method required fewer low-fidelity samples compared to mfEGRA and AMK-MCS+AEFF. These advantages make the proposed method a promising approach for handling reliability analysis problems.

Although the proposed method has proven effective for general reliability analysis problems, its use could be further extended to address hybrid reliability analysis problems that involve both random and interval variables. Moreover, the basic framework

of the proposed method could be enhanced by incorporating dimension reduction methods (Zhou and Peng, 2020; Ji et al., 2022) to address high-dimensional reliability analysis problems.

Acknowledgements

This work was supported by the Major Projects of Zhejiang Provincial Natural Science Foundation of China (No. LD22E050009), the National Natural Science Foundation of China (No. 51475425), and the College Student's Science and Technology Innovation Project of Zhejiang Province (No. 2022R403B060).

Author contributions

Yifan LI devised the methodology, developed the software, validated the results, and wrote the initial draft. Yongyong XIANG optimized the methodology and revised the manuscript. Luojie SHI optimized the software and revised the manuscript. Baisong PAN conceived the methodology and edited the final version.

Conflict of interest

Yifan LI, Yongyong XIANG, Luojie SHI, and Baisong PAN declare that they have no conflict of interest.

References

- Aldosary M, Wang J, Li CF, 2018. Structural reliability and stochastic finite element methods: State-of-the-art review and evidence-based comparison. *Engineering with Computers*, 35(6):2165-2214.
<https://doi.org/10.1108/EC-04-2018-0157>
- Bichon BJ, Eldred MS, Swiler LP, et al., 2008. Efficient global reliability analysis for nonlinear implicit performance functions. *AIAA Journal*, 46(10):2459-2468.
<https://doi.org/10.2514/1.34321>
- Chaudhuri A, Marques AN, Willcox K, 2021. mfEGRA: Multifidelity efficient global reliability analysis through active learning for failure

- boundary location. *Structural and Multidisciplinary Optimization*, 64(2):797-811.
<https://doi.org/10.1007/s00158-021-02892-5>
- Chen J, Gao Y, Liu YM, 2022. Multi-fidelity data aggregation using convolutional neural networks. *Computer Methods in Applied Mechanics and Engineering*, 391: 114490.
<https://doi.org/10.1016/j.cma.2021.114490>
- Cheng J, Li QS, 2008. Reliability analysis of structures using artificial neural network based genetic algorithms. *Computer Methods in Applied Mechanics and Engineering*, 197(45-48):3742-3750.
<https://doi.org/10.1016/j.cma.2008.02.026>
- Cutajar K, Pullin M, Damianou A, et al., 2019. Deep gaussian processes for multi-fidelity modeling. arXiv preprint, arXiv:1903.07320.
<https://doi.org/10.48550/arXiv.1903.07320>
- Echard B, Gayton N, Lemaire M, 2011. AK-MCS: an active learning reliability method combining Kriging and Monte Carlo simulation. *Structural Safety*, 33(2):145-54.
<https://doi.org/10.1016/j.strusafe.2011.01.002>
- Echard B, Gayton N, Lemaire M, et al., 2013. A combined importance sampling and kriging reliability method for small failure probabilities with time-demanding numerical models. *Reliability Engineering & System Safety*, 111: 232-240.
<https://doi.org/10.1016/j.ress.2012.10.008>
- Feng JW, Liu L, Wu D, et al., 2019. Dynamic reliability analysis using the extended support vector regression (X-SVR). *Mech Syst Signal Process* 126:368-391.
<https://doi.org/10.1016/j.ymsp.2019.02.027>
- Forrester AIJ, Sobester A, Keane AJ, 2007. Multi-fidelity optimization via surrogate modelling. *Proceedings of the Royal Society A: Mathematical, Physical and Engineering Sciences*, 463(2088):3251-3269.
<https://doi.org/10.1098/rspa.2007.1900>
- Forrester AIJ, Sobester A, Keane AJ, 2008. Engineering design via surrogate modelling: a practical guide. John Wiley & Sons.
- Gavin HP, Yau SC, 2008. High-order limit state functions in the response surface method for structural reliability analysis. *Structural Safety*, 30(2):162-179.
<https://doi.org/10.1016/j.strusafe.2006.10.003>
- Goswami S, Ghosh S, Chakraborty S, 2016. Reliability analysis of structures by iterative improved response surface method. *Structural Safety*, 60:56-66.
<https://doi.org/10.1016/j.strusafe.2016.02.002>
- Guo MW, Manzoni A, Amendt M, et al., 2022. Multi-fidelity regression using artificial neural networks: efficient approximation of parameter-dependent output quantities. *Computer Methods in Applied Mechanics and Engineering*, 389:114378.
<https://doi.org/10.1016/j.cma.2021.114378>
- He WX, Zeng Y, Li G, 2020. An adaptive polynomial chaos expansion for high-dimensional reliability analysis. *Structural and Multidisciplinary Optimization*, 62(4):2051-67.
<https://doi.org/10.1007/s00158-020-02594-4>
- Hohenbichler M, Rackwitz R, 1982. First-order concepts in system reliability. *Structural Safety*, 1(3):177-188.
[https://doi.org/10.1016/0167-4730\(82\)90024-8](https://doi.org/10.1016/0167-4730(82)90024-8)
- Hong HP, 1996. Point-estimate moment-based reliability analysis. *Civil Engineering Systems*, 13(4): 281-294.
<https://doi.org/10.1080/02630259608970204>
- Hong LX, Li HC, Fu JF, 2022. A novel surrogate-model based active learning method for structural reliability analysis. *Computer Methods in Applied Mechanics and Engineering*, 394: 114835.
<https://doi.org/10.1016/j.cma.2022.114835>
- Hu C, Youn BD, 2011. Adaptive-sparse polynomial chaos expansion for reliability analysis and design of complex engineering systems. *Structural and Multidisciplinary Optimization*, 43(3):419-442.
<https://doi.org/10.1007/s00158-010-0568-9>
- Ji YX, Xiao NC, Zhan HY, 2022. High dimensional reliability analysis based on combinations of adaptive Kriging and dimension reduction technique. *Quality and Reliability Engineering International*, 38(5):2566-2585.
<https://doi.org/10.1002/qre.3091>
- Jones DR, Schonlau M, Welch WJ, 1998. Efficient global optimization of expensive black-box functions. *Journal of Global optimization*, 13(4):455-492.
<https://doi.org/10.1023/A:1008306431147>
- Kaymaz I, 2005. Application of kriging method to

- structural reliability problems. *Structural Safety*, 27(2):133-151.
<https://doi.org/10.1016/j.strusafe.2004.09.001>
- Kennedy MC, O'Hagan A, 2000. Predicting the output from a complex computer code when fast approximations are available. *Biometrika*, 87(1):1-13.
<https://doi.org/10.1093/biomet/87.1.1>
- Kiureghian AD, Stefano MD, 1991. Efficient algorithm for second-order reliability analysis. *Journal of Engineering Mechanics*, 117(12):2904-2923.
[https://doi.org/10.1061/\(ASCE\)0733-9399\(1991\)117:12\(2904\)](https://doi.org/10.1061/(ASCE)0733-9399(1991)117:12(2904))
- Krige DG, 1951. A statistical approach to some basic mine valuation problems on the Witwatersrand. *Journal of the Southern African Institute of Mining and Metallurgy*, 52(6):119-139.
https://hdl.handle.net/10520/AJA0038223X_4792
- Le GL, Garnier J, 2014. Recursive co-kriging model for design of computer experiments with multiple levels of fidelity. *International Journal for Uncertainty Quantification*, 4(5):365-386.
<https://doi.org/10.1615/Int.J.UncertaintyQuantification.2014006914>
- Lelièvre N, Beaurepaire P, Mattrand C, et al., 2018. AK-MCSi: A Kriging-based method to deal with small failure probabilities and time-consuming models. *Structural Safety*, 73:1-11.
<https://doi.org/10.1016/j.strusafe.2018.01.002>
- Li HS, Cao ZJ, 2016. Matlab codes of Subset Simulation for reliability analysis and structural optimization. *Structural and Multidisciplinary Optimization*, 54(2):391-410.
<https://doi.org/10.1007/s00158-016-1414-5>
- Li MY, Wang ZQ, 2019. Surrogate model uncertainty quantification for reliability-based design optimization. *Reliability Engineering & System Safety*, 192:106432.
<https://doi.org/10.1016/j.ress.2019.03.039>
- Li X, Gong CL, Gu LX, et al., 2018. A sequential surrogate method for reliability analysis based on radial basis function. *Structural Safety*, 73:42-53.
<https://doi.org/10.1016/j.strusafe.2018.02.005>
- Liu J, Yi JX, Zhou Q, et al., 2020. A sequential multi-fidelity surrogate model-assisted contour prediction method for engineering problems with expensive simulations. *Engineering with Computers*, 38:31-49.
<https://doi.org/10.1007/s00366-020-01043-6>
- Lophaven SN, Nielsen HB, Sondergaard J, 2002. DACE, a matlab Kriging toolbox, version 2.0. Technical Report; IMM-TR-2002-12; Technical University of Denmark; 2002a.
<http://www2.imm.dtu.dk/hbn/dace/>
- Marques A, Lam R, Willcox K, 2018. Contour location via entropy reduction leveraging multiple information sources. *Advances in Neural Information Processing Systems*, 5217-5227.
- Melchers R, 1990. Radial importance sampling for structural reliability. *Journal of Engineering Mechanics*, 116(1):189-203.
[https://doi.org/10.1061/\(ASCE\)0733-9399\(1990\)116:1\(189\)](https://doi.org/10.1061/(ASCE)0733-9399(1990)116:1(189))
- Meng XH, Karniadakis G E, 2020. A composite neural network that learns from multi-fidelity data: Application to function approximation and inverse PDE problems. *Journal of Computational Physics*, 401: 109020.
<https://doi.org/10.1016/j.jcp.2019.109020>
- Papaioannou I, Papadimitriou C, Straub D, 2016. Sequential importance sampling for structural reliability analysis. *Structural Safety*, 62:66-75.
<https://doi.org/10.1016/j.strusafe.2016.06.002>
- Perdikaris P, Raissi M, Damianou A, et al., 2017. Nonlinear information fusion algorithms for data-efficient multi-fidelity modelling. *Proceedings of the Royal Society A: Mathematical, Physical and Engineering Sciences*, 473(2198):20160751.
<https://doi.org/10.1098/rspa.2016.0751>
- Rajashekhar MR, Ellingwood BR, 1993. A new look at the response surface approach for reliability analysis. *Structural Safety*, 12(3):205-220.
[https://doi.org/10.1016/0167-4730\(93\)90003-J](https://doi.org/10.1016/0167-4730(93)90003-J)
- Reisenthel PH, Allen TT, 2014. Application of multi-fidelity expected improvement algorithms to aeroelastic design optimization. 10th AIAA multidisciplinary design optimization conference 1490.
<https://doi.org/10.2514/6.2014-1490>
- Ren C, Aoues Y, Lemosse D, et al., 2022. Ensemble of surrogates combining Kriging and Artificial Neural Networks for reliability analysis with local goodness measurement. *Structural Safety*, 96:102186.

- <https://doi.org/10.1016/j.strusafe.2022.102186>
- Roy A, Manna R, Chakraborty S, 2019. Support vector regression based metamodeling for structural reliability analysis. *Probabilistic Engineering Mechanics*, 55:78-89.
<https://doi.org/10.1016/j.probenmech.2018.11.001>
- Schüßler GI, Pradlwarter HJ, 2007. Benchmark study on reliability estimation in higher dimensions of structural systems—an overview. *Structural Safety*, 29(3):167-182.
<https://doi.org/10.1016/j.strusafe.2006.07.010>
- Song SF, Lu ZZ, Qiao HW, 2009. Subset simulation for structural reliability sensitivity analysis. *Reliability Engineering & System Safety*, 94(2):658-665.
<https://doi.org/10.1016/j.res.2008.07.006>
- Su GS, Peng LF, Hu LH, 2017. A Gaussian process-based dynamic surrogate model for complex engineering structural reliability analysis. *Structural Safety*, 68:97-109.
<https://doi.org/10.1016/j.strusafe.2017.06.003>
- Wang JS, Li CF, Xu GJ, et al., 2021. Efficient structural reliability analysis based on adaptive Bayesian support vector regression. *Computer Methods in Applied Mechanics and Engineering*, 387:114172.
<https://doi.org/10.1016/j.cma.2021.114172>
- Wang ZY, Shafieezadeh A, 2019. REAK: Reliability analysis through Error rate-based Adaptive Kriging. *Reliability Engineering & System Safety*, 182: 33-45.
<https://doi.org/10.1016/j.res.2018.10.004>
- Wang ZY, Shafieezadeh A, 2019. ESC: an efficient error-based stopping criterion for kriging-based reliability analysis methods. *Structural and Multidisciplinary Optimization*, 59(5):1621-1637.
<https://doi.org/10.1007/s00158-018-2150-9>
- Wu HQ, Kuang SJ, Hou HB, 2019. Research on application of electric vehicle collision based on reliability optimization design method. *International Journal of Computational Methods*, 16(07):1950034.
<https://doi.org/10.1142/S0219876219500348>
- Yi JX, Wu FL, Zhou Q, et al., 2021. An active-learning method based on multi-fidelity Kriging model for structural reliability analysis. *Structural and Multidisciplinary Optimization*, 63(1):173-195.
<https://doi.org/10.1007/s00158-020-02678-1>
- Youn BD, Choi K, Yang RJ, et al., 2004. Reliability-based design optimization for crashworthiness of vehicle side impact. *Structural and Multidisciplinary Optimization*, 26(3):272-283.
<https://doi.org/10.1007/s00158-003-0345-0>
- Zhang XF, Pandey MD, 2013. Structural reliability analysis based on the concepts of entropy, fractional moment and dimensional reduction method. *Structural Safety*, 43: 28-40.
<https://doi.org/10.1016/j.strusafe.2013.03.001>
- Zhang XF, Wang L, Sørensen J D, 2020. AKOIS: an adaptive Kriging oriented importance sampling method for structural system reliability analysis. *Structural Safety*, 82: 101876.
<https://doi.org/10.1016/j.strusafe.2019.101876>
- Zhao H, Gao ZH, Xu F, et al., 2019. Review of robust aerodynamic design optimization for air vehicles. *Archives of Computational Methods in Engineering*, 26(3):685-732.
<https://doi.org/10.1007/s11831-018-9259-2>
- Zhou T, Peng YB, 2020. Kernel principal component analysis-based Gaussian process regression modelling for high-dimensional reliability analysis. *Computers and Structures*, 241:106358.
<https://doi.org/10.1016/j.compstruc.2020.106358>
- Zhou T, Peng YB, 2020. Structural reliability analysis via dimension reduction, adaptive sampling, and Monte Carlo simulation. *Structural and Multidisciplinary Optimization*, 62(5):2629-2651.
<https://doi.org/10.1007/s00158-020-02633-0>

Electronic supplementary materials

Sections S1 and S2

中文概要

题目: 基于非线性自回归多保真代理模型和主动学习的高效可靠性分析方法

作者: 李一帆, 项涌涌, 施罗杰, 潘柏松

机构: 浙江工业大学, 机械工程学院, 中国杭州, 310023

目的: 针对现有多保真建模方法需要嵌套训练样本来捕

捉数据相关性导致的计算成本增加与未充分考虑不同保真度样本之间非线性关系导致的模型精度低问题，本文提出了一种结合多保真建模和主动学习的可靠性分析方法，旨在实现高效且准确的失效概率估计。

创新点: 1. 基于非线性自回归方案并构建了一种非线性自回归多保真克里金 (NAMK) 模型; 2. 在模型更新过程中, 用集成的多保真学习函数代替传统的学习函数, 通过综合考虑采样成本和多保真样本之间的相关性, 从多保真样本空间中选择新的采样点; 3. 当选择高保真样本时, 使用残差模型生成嵌套的低保真样本。

方法: 1. 在指定的参数范围内选择初始多保真样本, 并使用 NAMK 构建初始代理模型; 2. 通过集成学习函数确定新样本的位置和保真度; 3. 一旦选择了一个高保真样本, 根据残差模型生成嵌套的低保真度样本并根据新的样本更新模型; 4. 使用基于相对误差估计的停止准则终止主动学习过程并输出失效概率估计结果。

结论: 1. 提出了一种基于多保真建模和主动学习的可靠分析方法, 提高了失效概率估计的效率和精度; 2. 利用 NAMK 模型来捕捉多保真样本之间的非线性关系, 有效提高了代理模型的准确性; 3. 考虑多保真样本的相关性和采样成本的学习函数能自适应地确定新样本的位置和保真度; 4. 当学习函数选择高保真样本时, 通过构造残差模型生成嵌套的低保真度样本, 减少了低保真度模型的调用次数。

关键词: 可靠性分析; 多保真代理模型; 主动学习; 非线性; 残差模型